Making Trotterization Adaptive and Energy-Self-Correcting for NISQ Devices and Beyond

Hongzheng Zhao,[1,*] Marin Bukov,[1,2] Markus Heyl,[1,3] and Roderich Moessner[1]

[1] *Max Planck Institute for the Physics of Complex Systems, Nöthnitzer Strasse 38, Dresden 01187, Germany*

[2] *Department of Physics, St. Kliment Ohridski University of Sofia, 5 James Bourchier Boulevard, Sofia 1164, Bulgaria*

[3] *Theoretical Physics III, Center for Electronic Correlations and Magnetism, Institute of Physics, University of Augsburg, Augsburg 86135, Germany*

(Received 26 January 2023; accepted 3 July 2023; published 9 August 2023)

Simulation of continuous-time evolution requires time discretization on both classical and quantum computers. A finer time step improves simulation precision but it inevitably leads to increased computational efforts. This is particularly costly for today's noisy intermediate-scale quantum computers, where notable gate imperfections limit the circuit depth that can be executed at a given accuracy. Classical adaptive solvers are well developed to save numerical computation times. However, it remains an outstanding challenge to make optimal usage of the available quantum resources by means of adaptive time steps. Here, we introduce a quantum algorithm to solve this problem, providing a controlled solution of the quantum many-body dynamics of local observables. The key conceptual element of our algorithm is a feedback loop that self-corrects the simulation errors by adapting time steps, thereby significantly outperforming conventional Trotter schemes on a fundamental level and reducing the circuit depth. It even allows for a controlled asymptotic long-time error, where the usual Trotterized dynamics faces difficulties. Another key advantage of our quantum algorithm is that any desired conservation law can be included in the self-correcting feedback loop, which has a potentially wide range of applicability. We demonstrate the capabilities by enforcing gauge invariance, which is crucial for a faithful and long-sought-after quantum simulation of lattice gauge theories. Our algorithm can potentially be useful on a more general level whenever time discretization is involved also concerning, e.g., numerical approaches based on time-evolving block-decimation methods.

DOI: 10.1103/PRXQuantum.4.030319

I. INTRODUCTION

Quantum computers hold the promise to outperform their classical counterparts in certain computational tasks. Among others, the emulation of quantum many-body systems in and out of equilibrium attracts considerable attention [1,2]. State-of-the-art quantum devices for digital quantum simulation (DQS), such as trapped ions [3–5], superconducting circuits [6–8], and Rydberg platforms [9–11], have recently realized condensed-matter models [12–22], simulation of molecular energies [23,24], and lattice gauge theories (LGTs) with the potential to answer long-standing questions in high-energy physics [25–32].

In this spirit, we consider a general quantum many-body system described by a Hamiltonian $H = \sum_{j=1}^{N} H_j$ with N terms, the dynamics of which we would like to simulate. In DQS, we assert that the time evolution generated by each individual term H_j can be implemented on the simulator but not the total Hamiltonian H. The difficulty in DQS arises from the noncommutativity $[H_i, H_j] \neq 0$ $(i \neq j)$, which is a defining feature of quantum mechanics. The basic idea behind DQS is to decompose the target time-evolution operator $U = \exp(-itH)$ into a series of elementary few-body quantum gates. Over a short time step δt, we can approximate U by the digitized $U_T(\delta t) = \prod_{j=1}^{N} \exp(-i\delta t H_j)$, a procedure known as Trotterization [33–47]. The noncommutativity of H_j gives rise to a Trotter error that increases in δt [37]; the longer the simulation time, the larger is the error. Higher-order corrections can be systematically suppressed by using a smaller step size δt. However, these come at the price of an increased depth of the gate sequence. Minimization of the circuit depth is key for present-day noisy intermediate-scale quantum (NISQ)

*hzhao@pks.mpg.de

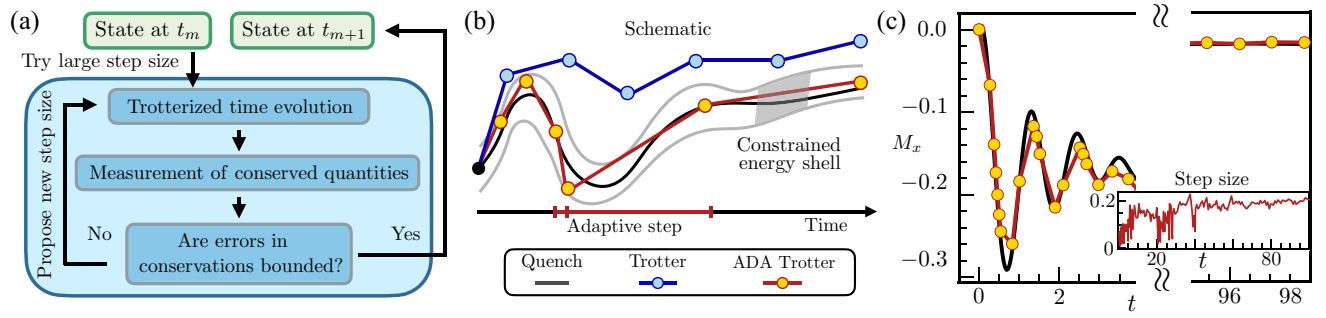

FIG. 1. (a) A schematic of the ADA Trotter protocol. Given a quantum state at time t_m and a Trotter expansion that approximates a target Hamiltonian, one tries to use the largest possible Trotter step size as long as errors in conservation laws are bounded. (b) ADA Trotter generally outperforms conventional Trotter: states propagated via ADA Trotter (orange) are constrained in a energy shell where energy and its variance are approximately conserved. In contrast, a fixed step size is chosen for conventional Trotter (blue) and larger errors may occur. (c) An illustration of the local dynamics obtained by ADA Trotter, which approximates the exact dynamics (black) closely at both short and long times. The inset shows the selected adaptive step size, which fluctuates in time. Smaller step sizes are chosen at early times to capture the rapid local oscillations, whereas an overall growing trend can be observed at longer times. We use $J_z = -1$, $h_x = -2$, $h_z = 0.2$, $L = 24$, and an initial state polarized in the negative y direction for our numerical simulations.

devices [2], which experience notable gate imperfections, with efficient quantum error correction still far out of reach [48–50]. By contrast, unlike in the case of classical computers, the physical (wall-clock) run time is at present not a similarly significant constraint. It is therefore a natural strategy to focus on minimizing the circuit depth, at fixed computation accuracy.

One way to do this is to introduce an adaptive Trotterization step size by exploiting the properties of the evolved state: e.g., at a fixed evolution time, a larger δt can give rise to a shorter gate sequence in time windows when the state changes slowly, without incurring a higher error. While this idea underlies adaptive solvers for differential equations and function-approximation techniques [51], promoting it to DQS requires addressing two formidable challenges. (i) Quantum states are not fully measurable; thus, it is *a priori* unclear which physical quantity should be used to produce a stable criterion that adapts the step size. (ii) By replacing continuous- with discrete-time evolution, Trotterization generally violates energy conservation. A variable step size removes even the remaining discrete-time translation invariance and hence opens further energy-absorption channels, manifest in increased approximation errors [52–55].

In this work, we propose an adaptive-step Trotterization scheme (ADA Trotter) for the DQS of many-body dynamics. We focus on time-independent Hamiltonians with arbitrary initial states, i.e., a setting corresponding to a generic quantum quench. We demonstrate that it outperforms conventional Trotterization while retaining a controllable error in local observables at all simulation times [56]. An essential element of our algorithm is a feedback loop that self-corrects the simulation errors in the conservation of the target Hamiltonian H, through adapting time steps, as summarized in Fig. 1. We derive a quantitative estimate of the long-time error for local observables and correlation functions. As a key result, we show that this error is independent of the simulation time and the number of qubits. While the feedback loop introduces an overhead for each performed time step, the additional resources required depend only polynomially, or logarithmically by using random measurements, on the system size. At the cost of a moderately increased run time on the quantum processor, ADA Trotter opens up the possibility of experimentally implementing accurate DQS beyond what is achievable with conventional Trotterization.

II. RESULTS

A. Adaptive Trotterization algorithm

Let us outline the ADA Trotter algorithm in detail [Fig. 1(a)]. The key idea behind it is to maximize a variable step size δt_m at each time t_m, while preserving the expectation value and the variance of the target Hamiltonian H, within some predefined fixed tolerances. Below, we show that other constraints, such as the preservation of symmetries, can also be imposed. We illustrate this by preserving gauge invariance, which can critically impact the accuracy of DQS for LGTs.

For a given quantum state $|\psi(t_m)\rangle$, we aim to find the largest possible time step δt_m such that, in the time-evolved state $|\psi(t_m+\delta t_m)\rangle = U_T(\delta t_m)|\psi(t_m)\rangle$, the energy density $\mathcal{E}_{m+1} = L^{-1}\langle\psi(t_m+\delta t_m)|H|\psi(t_m+\delta t_m)\rangle$ and the energy variance density $\delta\mathcal{E}^2_{m+1} = L^{-1}\langle\psi(t_m+\delta t_m)|H^2|\psi(t_m+\delta t_m)\rangle - L\mathcal{E}^2_{m+1}$ with the system size L both remain bounded:

$$|\mathcal{E}_{m+1} - \mathcal{E}| < d_{\mathcal{E}}, \qquad |\delta\mathcal{E}^2_{m+1} - \delta\mathcal{E}^2| < d_{\delta\mathcal{E}^2}, \quad (1)$$

where $\mathcal{E}$ and $\delta\mathcal{E}^2$ are the energy and variance density for the initial state. These conditions ensure the conservation of the average density and its fluctuations, up to the maximally allowed errors $d_{\mathcal{E}}$ and $d_{\delta\mathcal{E}^2}$. Crucially, as we always compare conserved quantities with their initial values, these errors will not accumulate in time. Remarkably, although we only constrain deviations in the lowest two moments of H explicitly, our numerical results suggest that it is sufficient to constrain the higher moments of H. Hence, the target Hamiltonian H emerges as an approximate constant of motion, despite Trotterization explicitly violating its conservation. While in conventional Trotterization the error is set by the step size, in ADA Trotter the error is controlled solely by the tolerances $d_{\mathcal{E}}$ and $d_{\delta\mathcal{E}^2}$.

The major challenge for ADA Trotter resides in capturing corrections to the dynamics beyond conventional Trotterization, which we control via a feedback loop that operates as follows [Fig. 1(a)]. First, a large time step δt_m is chosen. We implement the time evolution $U_T(\delta t_m)$ on the quantum processor, yielding a candidate state $|\tilde{\psi}(t_m + \delta t_m)\rangle = U_T(\delta t_m)|\psi(t_m)\rangle$. For this candidate state, we measure the energy density $\tilde{\mathcal{E}}_{m+1}$ and its fluctuations $\delta\tilde{\mathcal{E}}^2_{m+1}$, which can be accessed straightforwardly on quantum computers [57–59]. In the event that the measurement outcome violates the conditions of Eq. (1), a new smaller step size δt_m is proposed and this procedure starts over again.

Note that the state $|\psi(t_m)\rangle$ collapses after projective measurements and hence it needs to be regenerated. However, once the sequence of the step size before t_m has been determined, the actual run time for regeneration of the state is fast on most NISQ devices and determining the energy and its variance requires only polynomially many local measurements. By using classical shadows with random measurements [60–62], the measurement cost can be further improved to logarithmic dependence on the system sizes (see Sec. SM 2.5 in the Supplemental Material [63]).

An efficient way of finding a new suitable δt_m is the bisection method, although other search algorithms can also be employed (cf. the discussion regarding the search algorithm in Sec. SM 2.1 of the Supplemental Material [63]). Once a suitable δt_m has been found, we obtain the quantum state $|\psi(t_m + \delta t_m)\rangle$ at the next time step and repeat the procedure.

B. Classical emulation

Let us illustrate the ADA Trotter algorithm in a classical simulation. Although our algorithm is independent of the underlying model, for concreteness, we consider a nonintegrable quantum Ising model, $H = H_+ + H_-$, as our target Hamiltonian:

$$H_- = J_z \sum_j \sigma_j^z \sigma_{j+1}^z + h_z \sum_j \sigma_j^z, \quad H_+ = h_x \sum_j \sigma_j^x, \qquad (2)$$

for a chain of L lattice sites. We consider a uniform nearest-neighbor Ising coupling J_z and transverse and longitudinal fields h_x and h_z, respectively. Periodic boundary conditions are used unless otherwise specified. Without loss of generality, we employ a second-order Trotter-Suzuki decomposition, $U_T(\delta t) = e^{-i\delta t H_-/2} e^{-i\delta t H_+} e^{-i\delta t H_-/2}$, to represent the target time-evolution operator as a sequence of elementary gates.

As an example, in Fig. 1(c) we show the time evolution of the magnetization $M_x(t_m) = L^{-1}\sum_j \langle\sigma_j^x\rangle_m$ for an initial state polarized in the negative y direction; $\langle\cdots\rangle_m$ denotes the expectation in the state $|\psi(t_m)\rangle$. ADA Trotter (orange circles) closely approximates the exact solution (black). It not only correctly captures the early-time oscillations but also the relaxation of local observables at longer times. Details of the full time evolution and the performance gain compared with conventional Trotterization are discussed in Sec. SM 2.6 of the Supplemental Material [63]. The inset shows the adaptive step sizes, which can fluctuate by one order of magnitude, $\delta t_m \in [0.01, 0.46]$, demonstrating the flexibility and the advantage of the adaptive procedure. The bisection search method makes ten attempts on average before it can identify the optimal step size. Crucially, the attempt number does not scale up for larger system sizes, suggesting that the search algorithm can also be efficiently implemented on quantum processors with a large number of qubits (see discussions in Sec. SM 2.3 of the Supplemental Material [63]).

We now restrict the simulation to a maximum number of $N = 15$ Trotter steps; this is equivalent to limiting the circuit depth and it reflects constraints on present-day NISQ devices. Consider the initial state $\exp(-i\pi\sum_j \sigma_j^y/8)|\downarrow \ldots \downarrow\rangle$. The dynamics of the magnetization in the x and z directions are shown in Figs. 2(a) and 2(b), respectively. At early times, the exact dynamics (black) exhibit rapid oscillations in both observables, which damp out with time. For ADA Trotter with tight constraints in energy and variance, $d_{\mathcal{E}} = 0.03, d_{\delta\mathcal{E}^2} = 1$ (orange circles), the exact dynamics are reproduced with high accuracy. We include here both cases of a constrained energy variance with $d_{\delta\mathcal{E}^2} = 1$ and of an unconstrained variance $d_{\delta\mathcal{E}^2} = \infty$ (dashed red), to demonstrate the importance of preserving the second moment of energy.

ADA Trotter can outperform Trotterization with a fixed step size. To reach the same maximal physical simulation time ($t \approx 5.5$), we apply Trotterization with a fixed step size $\delta t = 0.36$ (green triangles), for which notable deviations in M_x already appear at very early times ($t \approx 1$); a smaller step size $\delta t = 0.16$ (blue diamonds) can be chosen to suppress local errors such that they are comparable to ADA Trotter. However, this comes at a cost of a reduced total simulated time ($t \approx 2.5$), which drops by a factor of 2 compared to ADA Trotter.

The reason behind the efficiency of ADA Trotter with tight constraints lies in the self-correction of errors in the

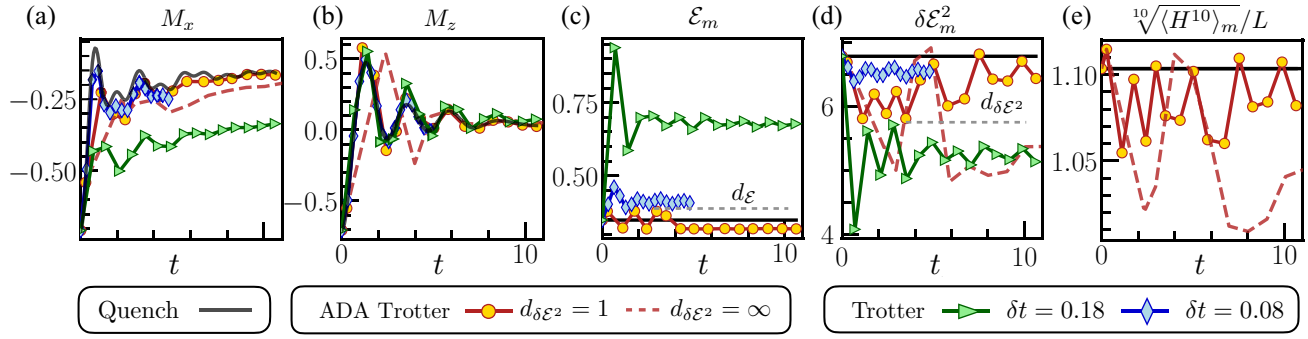

FIG. 2. A comparison between ADA Trotter and fixed-step Trotterization. (a) and (b) depict the time evolution of the magnetization in the x and z directions, respectively. The variance constraint is crucial for ADA Trotter: with variance constraint $d_{\delta\mathcal{E}^2}=1$ (orange circle), ADA Trotter reproduces the exact dynamics, whereas notable deviation appears for $d_{\delta\mathcal{E}^2}=\infty$ (dashed red) without variance control. ADA Trotter outperforms fixed-step Trotter: for a large fixed Trotter step ($\delta t=0.36$, green triangle), notable local errors appear at early times; a smaller δt can be employed (blue diamond) to suppress errors but the total simulation time is limited. (c) and (d) depict the expectation value of target Hamiltonian H and its variance, deviations of which are constrained by $d_\mathcal{E}$ and $d_{\delta\mathcal{E}^2}$ for ADA Trotter. Fixed-step Trotter can lead to a sufficiently large error in the energy at early times. (e) Higher moments of the target Hamiltonian are better preserved with the variance constraint. We use $J_z=-1$, $h_x=-1.7$, $h_z=0.5$, $d_\mathcal{E}=0.03$, and $L=24$ for our numerical simulations.

conservation law of the target Hamiltonian, a feature that is crucial for a faithful digital simulation but absent in the conventional Trotter scheme. As illustrated in Fig. 2(c), rather than being a conserved quantity (black), the energy density $\mathcal{E}_m$ now becomes time dependent for ADA Trotter (orange dots). Remarkably, it fluctuates around the correct value within a controlled error $d_\mathcal{E}$ (gray), signifying that our algorithm is self-correcting the energy errors by adapting the time steps. Similar behavior also occurs in the simulation shown in Fig. 1(c) (see details in Sec. SM 2.6 of the Supplemental Material [63]). In contrast, conventional Trotter (green) leads to notable deviations in energy, which saturate quickly at a value far from the black line and cannot be corrected.

At later times, the energy for ADA Trotter saturates in a preferred direction toward the center of the many-body spectrum ($\mathrm{Tr}[H]/L=0$) that corresponds to infinite temperature. This behavior is reminiscent of heating, which commonly occurs in time-dependent quantum chaotic systems where all initial states eventually reach infinite temperature due to energy absorption from the time-dependent drive [64–66]. However, the explicit constraints imposed in ADA Trotter [Eq. (1)] strictly forbid such a heat death.

Similarly, the energy variance also changes in time and notable deviation from the initial value (black line) can occur if there is no constraint in variance [$d_{\delta\mathcal{E}^2}=\infty$, dashed red line in Fig. 2(d)]. Such a deviation can be controlled by setting $d_{\delta\mathcal{E}^2}=1$ (orange circles) [67]. In Fig. 2(e), we show a higher moment of the target Hamiltonian $\sqrt[n]{\langle H^n\rangle_m}/L$ for $n=10$: remarkably, the errors in this quantity are also constrained at $d_{\delta\mathcal{E}^2}=1$ and grow with $d_{\delta\mathcal{E}^2}$. From this analysis, we conclude that enforcing only energy conservation is insufficient, while in addition constraining its variance is necessary to preserve the conservation of the target Hamiltonian. Similar behavior also occurs at the integrable point ($h_z=0$) (see Sec. SM 2.8 of the Supplemental Material [63]). It happens possibly because, by the central-limit theorem, the correct characterization of the energy distribution requires only the first two moments [68]. In particular, consider a Hamiltonian with nearest-neighboring interactions and a product state $|\psi(0)\rangle$ that are accessible on most current digital devices. Suppose that this state has mean energy E_0 and energy variance δE_0^2, such that the variance is lower bounded by the number of qubits $\delta E^2\geq aL$ with $a>0$: the energy distribution has been shown to converge to a Gaussian $\rho(E)\sim e^{-(E-E_0)^2/2\delta E^2}$ in the thermodynamic limit [68]. The condition can be easily verified as shown in Sec. SM 2.7 of the Supplemental Material [63]. In Sec. SM 2.8 of [63] we also fine tune the initial state such that it is far from a Gaussian distribution; hence, ADA Trotter may not perform well. However, we expect that the central-limit theorem should hold true for most generic realistic systems and states.

It is worth noting that the instantaneous long-time errors for ADA Trotter can be orders of magnitude smaller compared to the error at short times. For instance, in Fig. 2(a) with variance control (orange circles) at $t=1.2$, the error in M_x is close to 0.1, which drops to 0.004 at $t=5.5$; the same behavior occurs even without variance control (red dashed line). This is counterintuitive, since Trotter errors in the global wave function are expected to accumulate in time [46]. In the following, we will rationalize this observation with the help of the eigenstate-thermalization hypothesis (ETH) and derive a quantitative estimate for the ADA Trotter errors in local observables.

C. Control of asymptotic errors

In a standard quench setup, according to ETH, the long-time-averaged expectation value of a local observable O can be well captured by the diagonal-ensemble prediction [69]:

$$O_{\mathrm{diag}}(\mathcal{E}) \approx O(\mathcal{E}) + \frac{\delta\mathcal{E}^2}{2L} O''(\mathcal{E}). \tag{3}$$

Here, $O(\mathcal{E}) = \langle\mathcal{E}|O|\mathcal{E}\rangle$ is the microcanonical value for eigenstate $|\mathcal{E}\rangle$ at energy density $\mathcal{E}$. According to ETH, $O(\mathcal{E})$ is a smooth function of the energy density and $O''(\mathcal{E})$ denotes the second derivative with respect to $\mathcal{E}$. Usually, for locally interacting systems, the variance density $\delta\mathcal{E}^2$ does not scale with the system size; hence, the second contribution on the right-hand side vanishes in the thermodynamic limit ($L \to \infty$) [69].

For ADA Trotter, at long times, we assume that the system also reaches a diagonal ensemble at the shifted energy density $\mathcal{E} + d_{\mathcal{E}}$ and variance density $\delta\mathcal{E}^2 + d_{\delta\mathcal{E}^2}$. Then, one can perturbatively expand $O(\mathcal{E})$ in Eq. (3) in terms of $d_{\mathcal{E}}$ to estimate the local error for $L \to \infty$ as

$$O_{\mathrm{ada}} - O_{\mathrm{diag}}(\mathcal{E}) = d_{\mathcal{E}} O'(\mathcal{E}) + \frac{d_{\mathcal{E}}^2}{2} O''(\mathcal{E}) + \mathcal{O}(d_{\mathcal{E}}^3), \tag{4}$$

where $O_{\mathrm{ada}} = O_{\mathrm{diag}}(\mathcal{E} + d_{\mathcal{E}})$ denotes the diagonal-ensemble prediction for ADA Trotter. The explicit derivation is given in Appendix B. Equation (4) suggests a linear dependence on $d_{\mathcal{E}}$ either when $d_{\mathcal{E}}$ is small or when $O''(\mathcal{E})$ vanishes (see Fig. S18 in the Supplemental Material [63]). In Fig. 3(a), we show this error extracted from the long-time average of M_z as a function of $d_{\mathcal{E}}$ for different system sizes. The error bars correspond to the standard deviation of M_z in the large time window used to perform the time average (see details in Sec. SM 2.10 of [63]). Clearly, for a smaller $d_{\mathcal{E}}$, the local error decreases and vanishes in the limit $d_{\mathcal{E}} \to 0$ for large systems ($L \geq 18$). We also compute the deviation $O(\mathcal{E} + d_{\mathcal{E}}) - O(\mathcal{E})$ via exact diagonalization of the target Hamiltonian for $L = 20$, which matches well with the error in the time evolution in a large range of $d_{\mathcal{E}}$.

Our results imply that, for DQS of a quenched system in the thermodynamic limit, although variance deviations may introduce errors in ADA Trotter at early times (as shown in Fig. 2), they are suppressed by quantum thermalization at long times. A tight constraint in energy conservation suffices to bound errors in local observables asymptotically. This also holds true for correlation functions as long as ETH remains valid. By contrast, conventional Trotterization enters challenging regimes at long times and exhibits uncontrollable heating.

For any finite system size, however, errors in energy variance contribute to local observables. Understanding them is important, since many present-day DQS platforms are intermediate scale. These errors become particularly notable for $d_{\mathcal{E}} \ll d_{\delta\mathcal{E}^2}/L$, where the error is mostly generated by the variance deviation and one obtains $O_{\mathrm{ada}} - O_{\mathrm{diag}} \approx d_{\delta\mathcal{E}^2} O''(\mathcal{E})/2L$ (see more general discussions in Appendix B). In Fig. 3(b), we verify this linear dependence on $d_{\delta\mathcal{E}^2}/L$ in the asymptotic error on M_z for different $d_{\delta\mathcal{E}^2}$ and system sizes. Since it tends to cross the origin, this error becomes negligible for sufficiently large system sizes. We would also like to mention that, before reaching the tolerance in energy, a tight variance bound induces nontrivial transient dynamics with a constrained heating rate (see Sec. SM 2.9 of [63]).

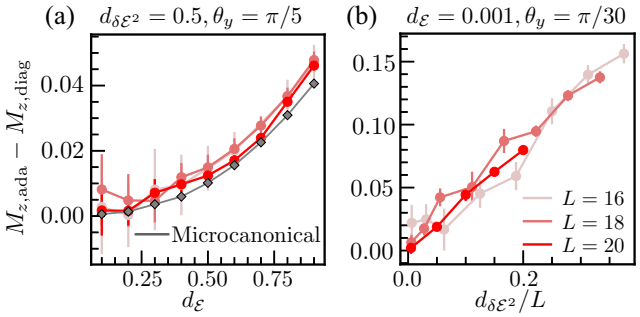

FIG. 3. The deviation in the expectation value for the z magnetization between the ADA Trotter and exact quench results in the long-time limit, as a function of (a) the energy-density deviation $d_{\mathcal{E}}$ and (b) the variance deviation $d_{\delta\mathcal{E}^2}$. (a) The local error decreases for a smaller energy deviation and can be captured by the microcanonical prediction (gray). (b) The variance deviation leads to local errors as finite-size effects, which vanish linearly in $d_{\delta\mathcal{E}^2}/L$. Parameters $J_z = 1$, $h_x = 1$, and $h_z = 0.3$ and initial states $\exp(-i\theta_y \sum_j \sigma_j^y)|\downarrow \ldots \downarrow\rangle$ are used for our numerical simulations.

D. Protection of gauge symmetry

One crucial generalization of ADA Trotter is to explicitly impose extra constraints in the feedback loop in addition to Eq. (1), such that other desired constants of motion can be preserved. This is impossible within the conventional Trotter scheme and independent of underlying models, highlighting the potential of ADA Trotter in DQS where symmetry is playing an important role. To illustrate this feature, we focus on protecting the local Gauss's law, which is crucial for LGTs and yet can easily be lost in real quantum simulators [25,27].

Consider the paradigmatic spin-S $U(1)$ quantum link model in $(1+1)$ dimensions, which is commonly used as a lattice version of quantum electrodynamics [30]. The model has two species of particles and can be described by

the Hamiltonian $H = H_{\text{kin}} + H_{\text{free}}$, with

$$H_{\text{kin}} = \sum_j \frac{J}{2\sqrt{S(S+1)}} \left(\sigma_j^+ s_{j,j+1}^+ \sigma_{j+1}^- + \text{h.c.}\right),$$
$$H_{\text{free}} = \sum_j \mu(-1)^j \sigma_j^z + k\left(s_{j,j+1}^z\right)^2. \quad (5)$$

Here, the spin-1/2 Pauli operator $\sigma_j^{\pm}$ creates or annihilates the matter field at site j; the $s_{j,j+1}$ operator represents the spin-S degree of freedom (DOF) positioned at the links between sites j and $j+1$; J is the kinetic energy term that couples the matter and gauge fields; μ denotes the bare-matter mass and k is the electric field coupling strength. We consider L matter sites and periodic boundary conditions. Gauss's law implies a U(1) gauge symmetry generated by the operator $G_j = \left[\sigma_j^z + s_{j-1,j}^z - s_{j,j+1}^z + (-1)^j\right]/2$, which commutes with the Hamiltonian H for any j. Therefore, the Hilbert space separates into exponentially many disconnected symmetry sectors. In the following, we focus on the sector satisfying Gauss's law, $G_j|\psi(0)\rangle = 0$, for any j, and use spin-1 gauge fields. Our method also applies for general spin-S DOF and other symmetry sectors, as discussed in Sec. SM 1.5 of the Supplemental Material [63].

We consider the initial state $|\psi(0)\rangle = |\uparrow\downarrow \ldots \uparrow\downarrow\rangle_\sigma \otimes |0\ldots 0\rangle_s$, fulfilling Gauss's law. To simulate the Trotterized time evolution, we consider for concreteness the decomposition $H_+ = H_{\text{kin}} + \lambda V$, $H_- = H_{\text{free}} - \lambda V$ with a gauge-breaking perturbation V. The average of H_+ and H_- reproduces the target Hamiltonian H. For zero perturbation strength λ, Gauss's law is ensured for all simulation times; for nonzero λ, the expectation value of the gauge generator $\mathcal{G}_m(j) = \langle G_j\rangle_m$ at site j, and its variance $\delta\mathcal{G}_m^2(j) = \langle G_j^2\rangle_m - \mathcal{G}_m^2(j)$ for the state $|\psi(t_m)\rangle$ obtained by ADA Trotter at time t_m, become time dependent and nonzero. To preserve the gauge symmetry, in addition to Eq. (1), we impose the conditions $\sum_j |\mathcal{G}_m(j)|/L < d_{\mathcal{G}}$, $\sum_j |\delta\mathcal{G}_m^2(j)|/L < d_{\delta\mathcal{G}^2}$, in the feedback loop to bound the density of the gauge violation.

In Figs. 4(a) and 4(b), respectively, we plot the errors in the expectation value of the gauge generator and its variance on a log scale. As the system involves both the matter and gauge d.o.f., the numerical simulation is limited to a small system size $L = 6$. Without constraints in gauge symmetry (blue line, $d_{\mathcal{G}} = \infty, d_{\delta\mathcal{G}^2} = \infty$), the errors in both panels increase quickly at short times and saturate around 0.1, indicating a severe violation of Gauss's law. By contrast, the additional constraint $d_{\mathcal{G}} = 0.001, d_{\delta\mathcal{G}^2} = 0.003$ (red line) significantly bounds the errors by 2 orders of magnitude and hence the gauge symmetry is controllably preserved.

The quick saturation of the errors measuring the violation of Gauss's law to a predefined tolerance (gray line) can cause ADA Trotter to "freeze" (i.e., the algorithm tends to always choose the smallest possible step size). Consequently, the quantum state barely propagates, despite the large number of quantum gates consumed. Freezing also occurs in quantum Ising models if the energy constraints are too tight. To resolve this issue, rather than using fixed tolerances, here we employ a soft constraint such that tolerances can increase by 30% of their original values whenever the smallest step size is chosen (for more details, see the Supplemental Material [63]).

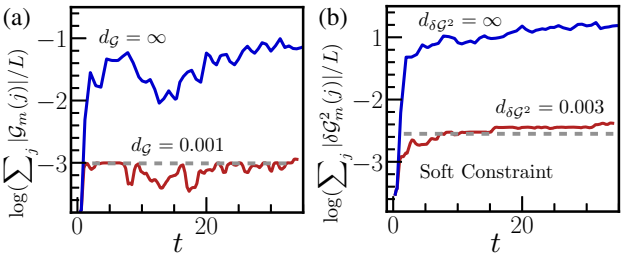

FIG. 4. The dynamics of the expectation values of the gauge symmetry generator in (a) and its variance in (b). Additional constraints on gauge violation preserve the gauge symmetry (red); otherwise errors grow quickly in a short time (blue). A soft constraint is used to prevent ADA Trotter from freezing. We use $J = 0.5$, $\mu = 0.5$, $k = 0.5$, $d_{\mathcal{E}} = 0.1$, $d_{\delta\mathcal{E}^2} = 0.2$, $\lambda = 0.3$, $L = 6$, and $V = \sum_j \left[s_{j,j+1}^+/\sqrt{S(S+1)} + \sigma_j^+\sigma_{j+1}^- + \text{h.c.}\right]$ for our numerical simulations.

III. DISCUSSION

The ADA Trotter algorithm that we propose is capable of simulating the local time evolution for DQS of time-independent systems, with controllable errors at all times. This adaptive and self-correcting scheme can be particularly useful when there are different time scales throughout the evolution, which typically happens as a result of quantum thermalization separating the early-time coherent oscillations and long-time relaxation. Furthermore, we find that quantum thermalization suppresses errors in local observables and ensures the long-time stability of ADA Trotter, which is absent in conventional Trotter, where systems normally exhibit uncontrollable heating to infinite temperature. It would be worth benchmarking ADA Trotter when thermalization is absent, e.g., when systems are integrable [70], long-range interacting [71], many-body localized [72], or host quantum many-body scars [73]. Those nonthermalizing systems normally have an extensive number of conserved quantities, for which extra constraints in the feedback loop may be required.

ADA Trotter remains robust and can still self-correct errors in energy even in the presence of dissipation, as long as the noise strength is weak (for more details, see Sec. SM 1.2 of [63]). It would also be interesting to use error mitigation to further improve the accuracy of this algorithm [74–78].

We generalize ADA Trotter to protect symmetries in addition to the energy constraints and we demonstrate this by controlling the violation of Gauss's law in U(1) LGTs. By preserving the time evolution in a given symmetry sector, ETH still applies and ADA Trotter remains stable at long times. Such symmetry protection is independent of the microscopic details of the target systems; hence, we expect it to have potentially a wide range of applicability. Note that such symmetry protection preserves the unitarity of the time evolution; hence, it is fundamentally different from postselection, which may introduce additional errors in DQS [28,31].

In practice, more sophisticated classical optimization routines may further improve the efficiency of ADA Trotter. For instance, Bayesian optimization can minimize the experimental efforts in measurement [79] and reinforcement learning may be useful in determining optimal step sizes and avoiding freezing [40,80–82].

Beyond DQS of quenched problems, Trotterization has been employed in other contexts, e.g., quantum imaginary time evolution [83], time-dependent Hamiltonian simulation [84–86], and classical numerical algorithms such as the time-evolving block-decimation method [87]. Our control scheme paves pathways to making these algorithms adaptive in time and improving their performance.

All data needed to evaluate the conclusions in the paper are present in the paper and/or the Supplemental Material [63]. Additional data and code are available on GitHub [88] or from the first author upon request.

ACKNOWLEDGMENTS

We thank Anatoli Polkovnikov, Johannes Knolle, Paul Schindler, Andrea Pizzi, Joseph Vovorsh, and Markus Drescher for enlightening discussions. This work is supported in part by the Deutsche Forschungsgemeinschaft under cluster of excellence ct.qmat (EXC 2147, project-id 390858490). M.B. was supported by the Marie Skłodowska-Curie Grant Agreement No. 890711. This project has received funding from the European Research Council (ERC) under the European Union Horizon 2020 research and innovation program (Grant Agreement No. 853443). This research was partially supported by the ARC DP210101367.

M.H. proposed the research. H.Z. proposed the algorithm and performed the analytical calculations and numerical simulations. All authors discussed the results and wrote the manuscript.

The authors declare that they have no competing interests.

APPENDIX A: NUMERICAL METHODS

We use the open-source PYTHON package QuSpin to perform exact diagonalization and quantum dynamics [89]. We employ a second-order Trotter-Suzuki decomposition, $U_T(\delta t) = e^{-i\delta t H_-/2} e^{-i\delta t H_+} e^{-i\delta t H_-/2}$, to realize the Trotterized time evolution. Numerically, the EXP_OP class in QuSpin is used, which does not calculate the actual matrix exponential of U_T but, instead, computes the action of the matrix exponential through its Taylor series. For translation-invariant systems, we restrict the basis in the zero-momentum block to enable the simulation of larger system sizes. If the system is parity symmetric with respect to the middle of the chain, we only use basis in the positive-parity sector. For the microcanonical prediction of local observables as shown in Fig. 3, we also perform exact diagonalization of the target Hamiltonian in the zero-momentum and positive-parity symmetry sector.

To determine the optimal Trotter step size δt for ADA Trotter, different search algorithms (bisection and sequential search) are used (for more details, see Sec. SM 2.1 of the Supplemental Material [63]). Bisection search is used to generate the results in Figs. 1 and 2 and sequential search is used for the other figures in the main text.

APPENDIX B: LONG-TIME STABILITY OF ADA TROTTER

Based on the ETH, we are able to estimate the long-time deviation in the expectation values of local observables, for two diagonal ensembles with different energy and energy variance. Both the energy and its variance are controllable with ADA Trotter. Consider a generic quantum many-body system satisfying ETH, given an initial state with mean and variance of energy

$$E = \langle H\rangle_0, \quad \delta E^2 = \langle H^2\rangle_0 - \langle H\rangle_0^2. \tag{B1}$$

As the Hamiltonian is time independent, both quantities will be conserved. For a normal short-ranged-interacting system, we have the following scaling [69]:

$$E \sim L, \quad \delta E^2 \sim L, \tag{B2}$$

where L represents the system size in one dimension. The following results can also be generalized to higher dimensions. For a local observable $\hat{O}$, we define $\bar{O}$ as the long-time average

$$\bar{O} = \frac{1}{\tau}\int_0^\tau dt \langle \hat{O}\rangle_t, \tag{B3}$$

where $\langle\cdots\rangle_t$ denotes the expectation in the state $|\psi(t)\rangle$. $\bar{O}$ can be captured by the diagonal-ensemble prediction as $\bar{O} = O_{\text{diag}} = \sum_m |c_m|^2 O_{mm}$, where the diagonal elements of the operator read as $O_{mm} = \langle m|O|m\rangle$, $c_m = \langle\psi(0)|m\rangle$ for initial state $|\psi(0)\rangle$. By assuming that O_{mm} is a continuous function that can be approximated by its thermal prediction $O(E)$, one can perform a perturbative expansion around the microcanonical prediction for the diagonal

ensemble as [69]

$$O_{\text{diag}} = \sum_m |c_m|^2 \Big[O(E) + (E_m - E)O'(E) + \frac{1}{2}(E_m - E)^2 O''(E) + \dots \Big] = O(E) + \frac{1}{2}(\delta E)^2 O''(E) + \dots, \tag{B4}$$

where the dependence on $O'(E)$ vanishes. Since energy is an extensive quantity, we can use the density of the energy $\mathcal{E} = E/L$, so the above equation becomes

$$O_{\text{diag}} = O(\mathcal{E}) + \frac{1}{2}\frac{\delta E^2}{L^2} O''(\mathcal{E}) + \dots . \tag{B5}$$

In the main text, we define the density of the energy variance as $\delta\mathcal{E}^2 = \delta E^2/L$; hence we obtain $O_{\text{diag}} = O(\mathcal{E}) + \delta\mathcal{E}^2 O''(\mathcal{E})/2L + \dots$, which leads to Eq. (3). For Eq. (B5), as long as

$$\frac{1}{2}\frac{\delta E^2}{L^2} O''(\mathcal{E}) \ll O(\mathcal{E}), \tag{B6}$$

one can approximate O_{diag} solely by $O(\mathcal{E})$. This is normally the case, since δE^2 scales linearly in system size L by making the assumption that there are no long-range connected correlations in the system [69]. Thus, $\delta E^2/L^2 \sim 1/L$, which vanishes in the thermodynamic limit, and the diagonal-ensemble prediction matches with the canonical prediction as $O_{\text{diag}}(\mathcal{E}) = O(\mathcal{E})$.

For ADA Trotter, suppose that the total energy reaches a tolerance bound

$$\widetilde{E} = E + \Delta_E, \quad \delta\widetilde{E}^2 = \delta E^2 + \Delta_{\delta E^2}. \tag{B7}$$

For the long-time relaxation, one can make a similar calculation of O_{ada} as the diagonal ensemble obtained by ADA Trotter at shifted energy and variance:

$$O_{\text{ada}} = O(\widetilde{E}) + \frac{1}{2}(\delta\widetilde{E})^2 O''(\widetilde{E}) + \dots . \tag{B8}$$

We can now Taylor expand Eq. (B8) via Eq. (B7):

$$\begin{aligned} O_{\text{ada}} &= O(E) + \Delta_E O'(E) + \frac{\Delta_E^2}{2} O''(E) + \frac{1}{2}\left[\delta E^2 + \Delta_{\delta E^2}\right] \\ &\quad \times \left[O''(E) + \Delta_E O'''(E)\right] + \dots \\ &= \left(O(E) + \frac{1}{2}\delta E^2 O''(E)\right) + \Delta_E O'(E) \\ &\quad + \frac{\Delta_E^2 + \Delta_{\delta E^2}}{2} O''(E) + \frac{\delta E^2 + \Delta_{\delta E^2}}{2}\Delta_E O'''(E) \\ &\quad + \dots \end{aligned} \tag{B9}$$

and the first two terms match with O_{diag} in Eq. (B4). One can now express the above equation using the energy density:

$$O_{\text{ada}} = O_{\text{diag}}(\mathcal{E}) + \frac{\Delta_E}{L} O'(\mathcal{E}) + \frac{\Delta_E^2 + \Delta_{\delta E^2}}{2L^2} O''(\mathcal{E}) + \frac{\delta E^2 + \Delta_{\delta E^2}}{2L^3}\Delta_E O'''(\mathcal{E}) + \dots . \tag{B10}$$

The tolerances, $\Delta_{E,\delta E^2}$, in ADA Trotter are tunable parameters. Therefore, as long as these prefactors in the above higher-order corrections drop to zero for $L \to \infty$, one can guarantee that the long-time relaxed local observable matches with the exact result $O_{\text{diag}}(\mathcal{E})$. For instance, $\Delta_{E,\delta E^2}$ can be chosen to be a small constant value that does not scale with the system size. However, for large system sizes, the ADA Trotter algorithm may freeze and the system barely propagates, which is inefficient, as many quantum gates are wasted. Instead, in our numerical simulations, we consider the density constraints $\Delta_E/L = d_{\mathcal{E}}$, $\Delta_{\delta E^2}/L = d_{\delta\mathcal{E}^2}$ with constants $d_{\mathcal{E},\delta\mathcal{E}^2}$. Equation (B10) thus reduces to

$$O_{\text{ada}} = O_{\text{diag}}(\mathcal{E}) + d_{\mathcal{E}} O'(\mathcal{E}) + \frac{d_{\mathcal{E}}^2 L^2 + d_{\delta\mathcal{E}^2} L}{2L^2} O''(\mathcal{E}) + \frac{\delta E^2 + d_{\delta\mathcal{E}^2} L}{2L^2} d_{\mathcal{E}} O'''(\mathcal{E}) + \dots . \tag{B11}$$

In the thermodynamic limit in one dimension, one obtains

$$\lim_{L\to\infty} O_{\text{ada}} = O_{\text{diag}}(\mathcal{E}) + d_{\mathcal{E}} O'(\mathcal{E}) + \frac{d_{\mathcal{E}}^2}{2} O''(\mathcal{E}) + \mathcal{O}(d_{\mathcal{E}}^3), \tag{B12}$$

leading to Eq. (4). This suggests that the long-time error in local observables in ADA Trotter is dominated by energy deviation. The variance deviation can be ignored in the thermodynamic limit if ETH holds true. Of course, it is still important to discuss its effects on finite-size systems. Suppose that we have a small deviation in energy satisfying $d_{\mathcal{E}} \ll d_{\delta\mathcal{E}^2}/L$. Then, Eq. (B11) reduces to

$$O_{\text{ada}} = O_{\text{diag}}(\mathcal{E}) + \frac{d_{\delta\mathcal{E}^2}}{2L} O''(\mathcal{E}), \tag{B13}$$

indicating a linear dependence on $d_{\delta\mathcal{E}^2}/L$ in the local error, which is verified in Fig. 3.

[1] I. M. Georgescu, S. Ashhab, and F. Nori, Quantum simulation, Rev. Mod. Phys. **86**, 153 (2014).

[2] J. Preskill, Quantum computing in the NISQ era and beyond, Quantum **2**, 79 (2018).

[3] R. Blatt and C. F. Roos, Quantum simulations with trapped ions, Nat. Phys. **8**, 277 (2012).

[4] C. Monroe, W. C. Campbell, L.-M. Duan, Z.-X. Gong, A. V. Gorshkov, P. Hess, R. Islam, K. Kim, N. M. Linke, and G. Pagano, *et al.*, Programmable quantum simulations of spin

systems with trapped ions, Rev. Mod. Phys. **93**, 025001 (2021).

[5] P. T. Dumitrescu, J. G. Bohnet, J. P. Gaebler, A. Hankin, D. Hayes, A. Kumar, B. Neyenhuis, R. Vasseur, and A. C. Potter, Dynamical topological phase realized in a trapped-ion quantum simulator, Nature **607**, 463 (2022).

[6] Y. Salathé, M. Mondal, M. Oppliger, J. Heinsoo, P. Kurpiers, A. Potočnik, A. Mezzacapo, U. Las Heras, L. Lamata, and E. Solano, *et al.*, Digital Quantum Simulation of Spin Models with Circuit Quantum Electrodynamics, Phys. Rev. X **5**, 021027 (2015).

[7] K. Satzinger, Y.-J. Liu, A. Smith, C. Knapp, M. Newman, C. Jones, Z. Chen, C. Quintana, X. Mi, and A. Dunsworth, *et al.*, Realizing topologically ordered states on a quantum processor, Science **374**, 1237 (2021).

[8] J. Dborin, V. Wimalaweera, F. Barratt, E. Ostby, T. E. O'Brien, and A. G. Green, Simulating groundstate and dynamical quantum phase transitions on a superconducting quantum computer (2022), arXiv preprint ArXiv:2205.12996.

[9] D. Jaksch, J. I. Cirac, P. Zoller, S. L. Rolston, R. Côté, and M. D. Lukin, Fast Quantum Gates for Neutral Atoms, Phys. Rev. Lett. **85**, 2208 (2000).

[10] M. Saffman, T. G. Walker, and K. Mølmer, Quantum information with Rydberg atoms, Rev. Mod. Phys. **82**, 2313 (2010).

[11] H. Levine, A. Keesling, A. Omran, H. Bernien, S. Schwartz, A. S. Zibrov, M. Endres, M. Greiner, V. Vuletić, and M. D. Lukin, High-Fidelity Control and Entanglement of Rydberg-Atom Qubits, Phys. Rev. Lett. **121**, 123603 (2018).

[12] M. Gärttner, J. G. Bohnet, A. Safavi-Naini, M. L. Wall, J. J. Bollinger, and A. M. Rey, Measuring out-of-time-order correlations and multiple quantum spectra in a trapped-ion quantum magnet, Nat. Phys. **13**, 781 (2017).

[13] A. Smith, M. Kim, F. Pollmann, and J. Knolle, Simulating quantum many-body dynamics on a current digital quantum computer, npj Quantum Inf. **5**, 1 (2019).

[14] K. A. Landsman, C. Figgatt, T. Schuster, N. M. Linke, B. Yoshida, N. Y. Yao, and C. Monroe, Verified quantum information scrambling, Nature **567**, 61 (2019).

[15] J. Sun, S. Endo, H. Lin, P. Hayden, V. Vedral, and X. Yuan, Perturbative quantum simulation (2021), arXiv preprint ArXiv:2106.05938.

[16] F. Barratt, J. Dborin, M. Bal, V. Stojevic, F. Pollmann, and A. G. Green, Parallel quantum simulation of large systems on small NISQ computers, npj Quantum Inf. **7**, 1 (2021).

[17] J. Han, W. Cai, L. Hu, X. Mu, Y. Ma, Y. Xu, W. Wang, H. Wang, Y. Song, and C.-L. Zou, *et al.*, Experimental Simulation of Open Quantum System Dynamics via Trotterization, Phys. Rev. Lett. **127**, 020504 (2021).

[18] W. A. de Jong, M. Metcalf, J. Mulligan, M. Płoskoń, F. Ringer, and X. Yao, Quantum simulation of open quantum systems in heavy-ion collisions, Phys. Rev. D **104**, L051501 (2021).

[19] L. Pastori, T. Olsacher, C. Kokail, and P. Zoller, Characterization and verification of Trotterized digital quantum simulation via Hamiltonian and Liouvillian learning (2022), arXiv preprint ArXiv:2203.15846.

[20] H. Kamakari, S.-N. Sun, M. Motta, and A. J. Minnich, Digital Quantum Simulation of Open Quantum Systems Using Quantum Imaginary-Time Evolution, PRX Quantum **3**, 010320 (2022).

[21] X. Mi, M. Ippoliti, C. Quintana, A. Greene, Z. Chen, J. Gross, F. Arute, K. Arya, J. Atalaya, and R. Babbush, *et al.*, Time-crystalline eigenstate order on a quantum processor, Nature **601**, 531 (2022).

[22] A. M. Green, A. Elben, C. H. Alderete, L. K. Joshi, N. H. Nguyen, T. V. Zache, Y. Zhu, B. Sundar, and N. M. Linke, Experimental Measurement of Out-of-Time-Ordered Correlators at Finite Temperature, Phys. Rev. Lett. **128**, 140601 (2022).

[23] P. J. O'Malley, R. Babbush, I. D. Kivlichan, J. Romero, J. R. McClean, R. Barends, J. Kelly, P. Roushan, A. Tranter, and N. Ding, *et al.*, Scalable Quantum Simulation of Molecular Energies, Phys. Rev. X **6**, 031007 (2016).

[24] S. McArdle, S. Endo, A. Aspuru-Guzik, S. C. Benjamin, and X. Yuan, Quantum computational chemistry, Rev. Mod. Phys. **92**, 015003 (2020).

[25] C. Schweizer, F. Grusdt, M. Berngruber, L. Barbiero, E. Demler, N. Goldman, I. Bloch, and M. Aidelsburger, Floquet approach to $\mathbb{Z}_2$ lattice gauge theories with ultracold atoms in optical lattices, Nat. Phys. **15**, 1168 (2019).

[26] H. Lamm, S. Lawrence, Y. Yamauchi, and N. Collaboration, *et al.*, General methods for digital quantum simulation of gauge theories, Phys. Rev. D **100**, 034518 (2019).

[27] B. Yang, H. Sun, R. Ott, H.-Y. Wang, T. V. Zache, J. C. Halimeh, Z.-S. Yuan, P. Hauke, and J.-W. Pan, Observation of gauge invariance in a 71-site Bose-Hubbard quantum simulator, Nature **587**, 392 (2020).

[28] J. Vovrosh and J. Knolle, Confinement and entanglement dynamics on a digital quantum computer, Sci. Rep. **11**, 1 (2021).

[29] W. L. Tan, P. Becker, F. Liu, G. Pagano, K. Collins, A. De, L. Feng, H. Kaplan, A. Kyprianidis, and R. Lundgren, *et al.*, Domain-wall confinement and dynamics in a quantum simulator, Nat. Phys. **17**, 742 (2021).

[30] J. Mildenberger, W. Mruczkiewicz, J. C. Halimeh, Z. Jiang, and P. Hauke, Probing confinement in a $\mathbb{Z}_2$ lattice gauge theory on a quantum computer (2022), arXiv preprint ArXiv:2203.08905.

[31] N. H. Nguyen, M. C. Tran, Y. Zhu, A. M. Green, C. H. Alderete, Z. Davoudi, and N. M. Linke, Digital Quantum Simulation of the Schwinger Model and Symmetry Protection with Trapped Ions, PRX Quantum **3**, 020324 (2022).

[32] N. Klco, A. Roggero, and M. J. Savage, Standard model physics and the digital quantum revolution: Thoughts about the interface, Reports on Progress in Physics **85**, 064301 (2022).

[33] M. Suzuki, General theory of fractal path integrals with applications to many-body theories and statistical physics, J. Math. Phys. **32**, 400 (1991).

[34] D. W. Berry, G. Ahokas, R. Cleve, and B. C. Sanders, Efficient quantum algorithms for simulating sparse Hamiltonians, Commun. Math. Phys. **270**, 359 (2007).

[35] D. Poulin, M. B. Hastings, D. Wecker, N. Wiebe, A. C. Doherty, and M. Troyer, The Trotter step size required for

accurate quantum simulation of quantum chemistry (2014), arXiv preprint ArXiv:1406.4920.

[36] R. Babbush, D. W. Berry, I. D. Kivlichan, A. Y. Wei, P. J. Love, and A. Aspuru-Guzik, Exponentially more precise quantum simulation of fermions in second quantization, New J. Phys. **18**, 033032 (2016).

[37] M. Heyl, P. Hauke, and P. Zoller, Quantum localization bounds Trotter errors in digital quantum simulation, Sci. Adv. **5**, eaau8342 (2019).

[38] A. Tranter, P. J. Love, F. Mintert, N. Wiebe, and P. V. Coveney, Ordering of Trotterization: Impact on errors in quantum simulation of electronic structure, Entropy **21**, 1218 (2019).

[39] C. Cirstoiu, Z. Holmes, J. Iosue, L. Cincio, P. J. Coles, and A. Sornborger, Variational fast forwarding for quantum simulation beyond the coherence time, npj Quantum Inf. **6**, 1 (2020).

[40] A. Bolens and M. Heyl, Reinforcement Learning for Digital Quantum Simulation, Phys. Rev. Lett. **127**, 110502 (2021).

[41] Y.-X. Yao, N. Gomes, F. Zhang, C.-Z. Wang, K.-M. Ho, T. Iadecola, and P. P. Orth, Adaptive Variational Quantum Dynamics Simulations, PRX Quantum **2**, 030307 (2021).

[42] S.-H. Lin, R. Dilip, A. G. Green, A. Smith, and F. Pollmann, Real- and Imaginary-Time Evolution with Compressed Quantum Circuits, PRX Quantum **2**, 010342 (2021).

[43] J. Richter and A. Pal, Simulating Hydrodynamics on Noisy Intermediate-Scale Quantum Devices with Random Circuits, Phys. Rev. Lett. **126**, 230501 (2021).

[44] R. Mansuroglu, T. Eckstein, L. Nützel, S. A. Wilkinson, and M. J. Hartmann, Variational Hamiltonian simulation for translational invariant systems via classical pre-processing, arXiv e-prints, arXiv (2021).

[45] C. M. Keever and M. Lubasch, Classically optimized Hamiltonian simulation, arXiv preprint (2022), ArXiv:2205.11427.

[46] M. S. Tepaske, D. Hahn, and D. J. Luitz, Optimal compression of quantum many-body time evolution operators into brickwall circuits (2022), arXiv preprint ArXiv:2205.03445.

[47] Z.-J. Zhang, J. Sun, X. Yuan, and M.-H. Yung, Low-Depth Hamiltonian Simulation by an Adaptive Product Formula, Phys. Rev. Lett. **130**, 040601 (2023).

[48] L. Postler, S. Heuβen, I. Pogorelov, M. Rispler, T. Feldker, M. Meth, C. D. Marciniak, R. Stricker, M. Ringbauer, and R. Blatt, *et al.*, Demonstration of fault-tolerant universal quantum gate operations, Nature **605**, 675 (2022).

[49] S. Krinner, N. Lacroix, A. Remm, A. Di Paolo, E. Genois, C. Leroux, C. Hellings, S. Lazar, F. Swiadek, and J. Herrmann, *et al.*, Realizing repeated quantum error correction in a distance-three surface code, Nature **605**, 669 (2022).

[50] E. H. Chen, T. J. Yoder, Y. Kim, N. Sundaresan, S. Srinivasan, M. Li, A. D. Córcoles, A. W. Cross, and M. Takita, Calibrated Decoders for Experimental Quantum Error Correction, Phys. Rev. Lett. **128**, 110504 (2022).

[51] J. C. Butcher, *The Numerical Analysis of Ordinary Differential Equations: Runge-Kutta and General Linear Methods* (Wiley-Interscience, USA, 1987).

[52] P. T. Dumitrescu, R. Vasseur, and A. C. Potter, Logarithmically Slow Relaxation in Quasiperiodically Driven Random Spin Chains, Phys. Rev. Lett. **120**, 070602 (2018).

[53] D. V. Else, W. W. Ho, and P. T. Dumitrescu, Long-Lived Interacting Phases of Matter Protected by Multiple Time-Translation Symmetries in Quasiperiodically Driven Systems, Phys. Rev. X **10**, 021032 (2020).

[54] H. Zhao, F. Mintert, R. Moessner, and J. Knolle, Random Multipolar Driving: Tunably Slow Heating through Spectral Engineering, Phys. Rev. Lett. **126**, 040601 (2021).

[55] D. M. Long, P. J. Crowley, and A. Chandran, Many-body localization with quasiperiodic driving, Phys. Rev. B **105**, 144204 (2022).

[56] Infidelity in the global wave function can also be used to quantify the accuracy of DQS. However, it is not suitable for our purpose because, for many-body systems, infidelity significantly overestimates actual errors in local observables.

[57] C. Kokail, C. Maier, R. van Bijnen, T. Brydges, M. K. Joshi, P. Jurcevic, C. A. Muschik, P. Silvi, R. Blatt, and C. F. Roos, *et al.*, Self-verifying variational quantum simulation of lattice models, Nature **569**, 355 (2019).

[58] X. Mi, P. Roushan, C. Quintana, S. Mandra, J. Marshall, C. Neill, F. Arute, K. Arya, J. Atalaya, and R. Babbush, *et al.*, Information scrambling in quantum circuits, Science **374**, 1479 (2021).

[59] P. Naldesi, A. Elben, A. Minguzzi, D. Clément, P. Zoller, and B. Vermersch, Fermionic correlation functions from randomized measurements in programmable atomic quantum devices (2022), arXiv preprint ArXiv:2205.00981.

[60] H.-Y. Huang, R. Kueng, and J. Preskill, Predicting many properties of a quantum system from very few measurements, Nat. Phys. **16**, 1050 (2020).

[61] H.-Y. Huang, R. Kueng, and J. Preskill, Efficient Estimation of Pauli Observables by Derandomization, Phys. Rev. Lett. **127**, 030503 (2021).

[62] A. Elben, S. T. Flammia, H.-Y. Huang, R. Kueng, J. Preskill, B. Vermersch, and P. Zoller, The randomized measurement toolbox, Nat. Rev. Phys. **5**, 9 (2023).

[63] See the Supplemental Material at http://link.aps.org/supplemental/10.1103/10.1103/PRXQuantum.4.030319 for additional simulation with different initial states and physical models and more technical details for ADA Trotter.

[64] A. Lazarides, A. Das, and R. Moessner, Equilibrium states of generic quantum systems subject to periodic driving, Phys. Rev. E **90**, 012110 (2014).

[65] F. Machado, G. D. Kahanamoku-Meyer, D. V. Else, C. Nayak, and N. Y. Yao, Exponentially slow heating in short and long-range interacting Floquet systems, Phys. Rev. Res. **1**, 033202 (2019).

[66] A. Rubio-Abadal, M. Ippoliti, S. Hollerith, D. Wei, J. Rui, S. Sondhi, V. Khemani, C. Gross, and I. Bloch, Floquet Prethermalization in a Bose-Hubbard System, Phys. Rev. X **10**, 021044 (2020).

[67] By contrast, for fixed-step Trotterization, large deviations in energy and variance appear at very early times ($t \approx 1$) for $\delta t = 0.18$ (green triangle) shown in Figs. 2(c) and 2(d). Therefore, although Floquet theory suggests that the Floquet Hamiltonian H_F defined through the relation $U_T(\delta t) = \exp(-iH_F\delta t)$ is quasiconserved [37,90], H_F can still significantly deviate from the target Hamiltonian and induce notable local errors in DQS.

[68] M. Hartmann, G. Mahler, and O. Hess, Gaussian quantum fluctuations in interacting many particle systems, Lett. Math. Phys. **68**, 103 (2004).
[69] M. Rigol, V. Dunjko, and M. Olshanii, Thermalization and its mechanism for generic isolated quantum systems, Nature **452**, 854 (2008).
[70] F. H. Essler and M. Fagotti, Quench dynamics and relaxation in isolated integrable quantum spin chains, J. Stat. Mech.: Theory Exp. **2016**, 064002 (2016).
[71] S. Sugimoto, R. Hamazaki, and M. Ueda, Eigenstate Thermalization in Long-Range Interacting Systems, Phys. Rev. Lett. **129**, 030602 (2022).
[72] D. A. Abanin, E. Altman, I. Bloch, and M. Serbyn, Colloquium: Many-body localization, thermalization, and entanglement, Rev. Mod. Phys. **91**, 021001 (2019).
[73] M. Serbyn, D. A. Abanin, and Z. Papić, Quantum many-body scars and weak breaking of ergodicity, Nat. Phys. **17**, 675 (2021).
[74] S. Endo, Q. Zhao, Y. Li, S. Benjamin, and X. Yuan, Mitigating algorithmic errors in a Hamiltonian simulation, Phys. Rev. A **99**, 012334 (2019).
[75] Y. Yang, B.-N. Lu, and Y. Li, Accelerated Quantum Monte Carlo with Mitigated Error on Noisy Quantum Computer, PRX Quantum **2**, 040361 (2021).
[76] X.-M. Zhang, Z. Huo, K. Liu, Y. Li, and X. Yuan, Unbiased random circuit compiler for time-dependent Hamiltonian simulation (2022), arXiv preprint ArXiv:2212.09445.
[77] R. Takagi, S. Endo, S. Minagawa, and M. Gu, Fundamental limits of quantum error mitigation, npj Quantum Inf. **8**, 114 (2022).
[78] Y. Yang, A. Christianen, S. Coll-Vinent, V. Smelyanskiy, M. C. Bañuls, T. E. O'Brien, D. S. Wild, and J. I. Cirac, Simulating prethermalization using near-term quantum computers (2023), arXiv preprint ArXiv:2303.08461.
[79] F. Sauvage and F. Mintert, Optimal Quantum Control with Poor Statistics, PRX Quantum **1**, 020322 (2020).
[80] M. Bukov, A. G. Day, D. Sels, P. Weinberg, A. Polkovnikov, and P. Mehta, Reinforcement Learning in Different Phases of Quantum Control, Phys. Rev. X **8**, 031086 (2018).
[81] M. Y. Niu, S. Boixo, V. N. Smelyanskiy, and H. Neven, Universal quantum control through deep reinforcement learning, npj Quantum Inf. **5**, 1 (2019).
[82] M. M. Wauters, E. Panizon, G. B. Mbeng, and G. E. Santoro, Reinforcement-learning-assisted quantum optimization, Phys. Rev. Res. **2**, 033446 (2020).
[83] M. Motta, C. Sun, A. T. Tan, M. J. O'Rourke, E. Ye, A. J. Minnich, F. G. Brandão, and G. K. Chan, Determining eigenstates and thermal states on a quantum computer using quantum imaginary time evolution, Nat. Phys. **16**, 205 (2020).
[84] D. Poulin, A. Qarry, R. Somma, and F. Verstraete, Quantum Simulation of Time-Dependent Hamiltonians and the Convenient Illusion of Hilbert Space, Phys. Rev. Lett. **106**, 170501 (2011).
[85] J. W. Z. Lau, K. Bharti, T. Haug, and L. C. Kwek, Noisy intermediate scale quantum simulation of time dependent Hamiltonians (2021), arXiv preprint ArXiv:2101.07677.
[86] J. Watkins, N. Wiebe, A. Roggero, and D. Lee, Time-dependent Hamiltonian simulation using discrete clock constructions (2022), arXiv preprint ArXiv:2203.11353.
[87] U. Schollwöck, The density-matrix renormalization group in the age of matrix product states, Ann. Phys. (NY) **326**, 96 (2011).
[88] https://github.com/ZhaoHongzheng/ADA-Trotter
[89] P. Weinberg and M. Bukov, QuSpin: A PYTHON package for dynamics and exact diagonalisation of quantum many body systems part I: Spin chains, SciPost Phys. **2**, 003 (2017).
[90] T. Kuwahara, T. Mori, and K. Saito, Floquet-Magnus theory and generic transient dynamics in periodically driven many-body quantum systems, Ann. Phys. (NY) **367**, 96 (2016).